Amyloid β-peptides

How to cite:
International Edition: doi.org/10.1002/anie.202109758
German Edition: doi.org/10.1002/ange.202109758

A Water-Soluble Peptoid Chelator that Can Remove Cu^{2+} from Amyloid-β Peptides and Stop the Formation of Reactive Oxygen Species Associated with Alzheimer's Disease

Anastasia E. Behar, Laurent Sabater, Maria Baskin, Christelle Hureau, and Galia Maayan**

Abstract: *Cu bound to amyloid-β (Aβ) peptides can act as a catalyst for the formation of reactive oxygen species (ROS), leading to neuropathologic degradation associated with Alzheimer's disease (AD). An excellent therapeutic approach is to use a chelator that can selectively remove Cu from Cu–Aβ. This chelator should compete with Zn^{2+} ions (Zn) that are present in the synaptic cleft while forming a nontoxic Cu complex. Herein we describe* ***P3****, a water-soluble peptidomimetic chelator that selectively removes Cu^{2+} from Cu–Aβ in the presence of Zn and prevent the formation of ROS even in a reductive environment. We demonstrate, based on extensive spectroscopic analysis, that although* ***P3*** *extracts Zn from Cu,Zn–Aβ faster than it removes Cu, the formed Zn complexes are kinetic products that further dissociate, while Cu****P3*** *is formed as an exclusive stable thermodynamic product. Our unique findings, combined with the bioavailability of peptoids, make* ***P3*** *an excellent drug candidate in the context of AD.*

Introduction

Copper ions are key elements in the structure and function of natural biopolymers,[1] however, their overloading can be potentially toxic to living cells and may cause oxidative stress, cardiovascular disorders and neurodegenerative diseases including Alzheimer's disease (AD).[2] A known approach towards the development of therapeutics for AD is Cu-chelation.[3] The amyloid cascade hypothesis proposes that copper ions (Cu) play a harmful role in the excessive accumulation of a peptide called amyloid-β (Aβ),[4] which is associated with AD. In addition, it was previously shown that Cu-Aβ complex can catalyze the incomplete reduction of dioxygen by ascorbate as a reduction agent, leading to formation of reactive oxygen species (ROS), namely, superoxide $O_2^{\cdot-}$, hydrogen peroxide H_2O_2 and hydroxyl radical $HO^{\cdot}$.[3c] Therefore, removal of Cu-ions from Cu-Aβ complex could be one of the possible therapeutic approaches to prevent this process.[5] However, an important prerequisite for any chelator for Cu in context of AD, is not only the ability to compete with Aβ on Cu binding in order to prevent Cu-Aβ complex from catalyzing the production of ROS, but also to form a new Cu-chelator complex that is unable to catalyze formation of ROS on its own.[3b]

Although Zn^{2+} ions do not lead to the production of ROS, their concentration in the synaptic cleft is higher than the concentration of Cu,[6] making them more available for coordination than Cu. Moreover, as the Aβ affinity to Zn^{2+} is relatively lower than its affinity to Cu (at neutral pH, $K_A(Zn^{2+}\text{-A}\beta) = 10^5\text{–}10^6\ M^{-1}$,[3d,7] $K_A(Cu^{2+}\text{-A}\beta) = 10^9\text{–}10^{10}\ M^{-1}$ [8] and $K_A(Cu^{+}\text{-A}\beta) = 10^7\text{–}10^{10}\ M^{-1}$ [9]), it is possible that the examined Cu chelator will extract the Zn^{2+} ions from Aβ rather than extracting the Cu^{2+} ions from the toxic Cu-Aβ complex, thus hindering the inhibition of ROS production.[3b,10] Therefore, an ideal candidate for copper chelating towards the development of potential therapeutics for AD, should: (i) have an affinity towards Cu, which is high enough in order to extract Cu from Cu-Aβ but not too high to withdraw Cu from other essential metalloproteins,[3b,5e,f,9,11] (ii) have high selectivity to Cu over Zn,[3b,10] and (iii) not lead to the production of ROS (Scheme 1).[3b]

Although the usefulness of targeting Cu in the context of AD was questionned,[12] with the strongest argument being that none of the promising ligands studied in vitro show any clinical benefit, the criteria to be fulfilled by the chelators are continuously refined,[3b] while improvement of the chelators is nurtured by in vitro studies.[13,14] Despite a growing number of studies reporting on new Cu chelators, many challenges remain in order for these chelators to be developed as efficient drugs.[3b] This is because such chelators should meet several requirements including appropriate affinity and selectivity towards the targeted metal ion(s), good kinetic and stability properties, redox inertness together with blood–

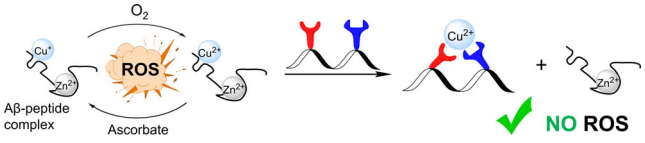

Scheme 1. Representation of a metal chelator designed to selectively extract Cu ions from Aβ–peptide complex, associated with ROS production in the context of AD.

[*] A. E. Behar, Dr. M. Baskin, Prof. Dr. G. Maayan
Schulich Faculty of Chemistry, Technion—Israel Institute of Technology
Technion City, 3200008 Haifa (Israel)
E-mail: gm92@technion.ac.il
Dr. L. Sabater, Dr. C. Hureau
CNRS; LCC (Laboratoire de Chimie de Coordination)
205 route de Narbonne, 31077 Toulouse (France)
and
Université de Toulouse
31077 Toulouse (France)
E-mail: christelle.hureau@lcc-toulouse.fr

Supporting information and the ORCID identification number(s) for the author(s) of this article can be found under: https://doi.org/10.1002/anie.202109758.

brain barrier (BBB) permeability and low toxicity.[3b] Small molecules Cu chelators, for example, are usually highly toxic, lead to a wide range of side effects, are unable to cross cell membranes and can only reach their target in the extracellular regions.[15] Peptide-based drugs can overcome some of these problems, but have other disadvantages: they typically show low BBB penetrability due to their large size, polarity and large number of hydrogen bond donors/acceptors, have short half-lives as well as low bioavailability, and they exhibit proteolytic instability and rapid clearance.[16] Thus, it is desirable to develop a unique type of chelators, preferably peptidomimetic-based ones that can combine the advantages of both small molecules and peptide-based drug candidates.

Peptoids[17], *N*-Substituted glycine oligomers, are excellent candidates for the development of metal chelators as potential therapeutics for AD: they can be easily synthesized on a solid support by the submonomer approach,[18] which utilizes primary amines as building blocks and thus allows to introduce a variety of functional groups within the peptoid sequence,[19] they are able to fold into well-defined secondary structures in solution,[20] and could be employed in various biological activities including protein-protein interactions,[21] metal binding and recognition,[22] and catalysis.[23] Moreover, compared to peptides, peptoids exhibit high proteolytic resistance[24] and high membrane permeability,[16a] together with tolerance towards high salts concentration and various pH conditions. In addition, some studies on the application of peptoids (not as chelators) towards AD therapy were previously reported and these were focused on inhibiting Aβ-peptide aggregation rather than on the arrest of ROS production.[25]

We have recently described the helical peptoid chelator **Helix HQT i+3** (**P1**, Figure 1 A), which is a hexamer incorporating a 8-hydroxyquinoline (HQ) group and a 2,2′:6′,2″-Terpyridine (Terpy) group at the 2nd and 5th positions, and (*S*)-(+)-1-phenylethylamine (Nspe) groups at the other positions.[26] **P1** shows high selectivity to Cu^{2+}, and can extract it from a methanolic solution containing 20 folds of similar metal ions such as Zn^{2+} and Co^{2+}.[26] We found that a primary request for this exceptional selectivity is the helicity of the peptoid with the two binding groups placed on the same side of the helix. The helical structure of **P1** was maintained via the four bulky chiral Nspe groups incorporated in addition within its sequence.[26] As a result, **P1** is hydrophobic and water insoluble, properties that limit its utilization as a drug candidate, despite its selectivity to Cu^{2+}. Interestingly, we have recently shown that the incorporation of one or more piperazine units within the backbone of hydrophobic peptoids ensures their water-solubility, while maintaining their sequence and structure.[27] Capitalizing on these findings, we present here a new, water-soluble and helical peptoid chelator, which is selective for Cu^{2+}, and describe how we applied it for the removal of Cu^{2+} from Aβ peptides, in aqueous medium, in order to stop the formation of ROS associated with AD, including in presence of Zn^{2+}.

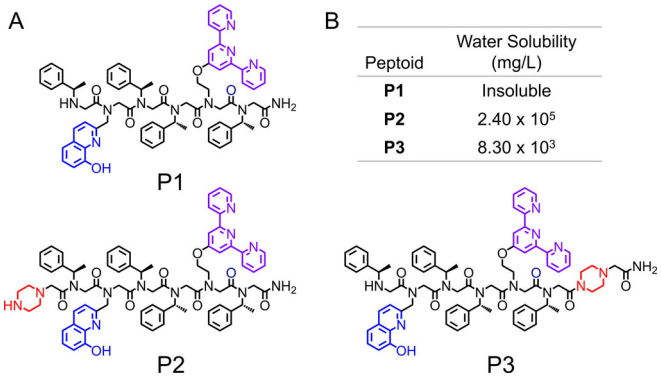

Peptoid	Water Solubility (mg/L)
P1	Insoluble
P2	2.40 x 10^5
P3	8.30 x 10^3

Figure 1. Selective binding of Cu^{2+} in water: A) sequences of peptoid chelators **P1**–**P3**. B) Water solubility data for **P1**–**P3** at pH 7.0.

Results and Discussion

Synthesis and Selectivity of Water-Soluble Hydrophobic Peptoid Chelator

Our first goal was to explore whether our highly selective peptoid chelator described above (**Helix HQT i+3** or **P1**, Figure 1 A), which is insoluble in water, can become water-soluble upon the addition of one or two piperazine groups at the N- or C-terminals of its sequence while maintaining its selectivity to Cu^{2+} in water. To this aim, we have synthesized two peptoids based on **P1**, by incorporating only one piperazine group at either its N- or C-terminus, forming **P2** and **P3**, respectively (Figure 1 and Figure S1 to S6). Circular dichroism (CD) measurements of both peptoids in water resulted in spectra that exhibit double minima near 208 and 220 nm, characteristic of Nspe-based peptoid helix, indicating that both peptoids preserve their helical secondary structure in water (Figure S7). In order to evaluate the selectivity of **P2** and **P3** towards Cu^{2+} from a mixture solution containing 1 equiv of Cu^{2+} ions and 1 equiv of the metal ions Co^{2+}, Zn^{2+}, Fe^{3+}, Mn^{2+} and Ni^{2+}, 1 equiv of this mixture was added to 1 equiv of each peptoid in un-buffered water and the UV/Vis spectra was recorded. The obtained UV/Vis spectrum in the case of **P2** was different from the spectrum of its copper complex (Figure S8, left) suggesting that there is no selective binding to Cu^{2+} by **P2.**[26] In contrast, the UV/Vis spectrum obtained in the case of **P3** was identical to the spectrum of its copper complex (Figure S8, right) implying a selective binding in this case. This selective binding was further supported by MS studies of solutions containing either **P3** and Cu or **P3** with a mixture of metal ions (Figure S9–13). These apparent conflicting results may be attributed to the ability of piperazine, when incorporated at the N-terminus, to participate in the binding of some metal ions and disable the unique coordination geometry of the Cu^{2+} complex that allows its selective binding.[26] Therefore, we can conclude that the addition of one piperazine group at the C-terminus of **P1**, leads to its water-soluble analogue **P3**, while maintaining both the hydrophobic sequence of **P1**, its helical structure and its fairly high selectivity to Cu^{2+}, but this time in aqueous solution.

Binding of P3 to Cu^{2+}

In un-buffered water (pH 7.0), metal-free **P3** exhibits absorption bands near $\lambda = 246$ and 279 nm, arising from the ligands HQ and Terpy, respectively. Upon addition of Cu^{2+} ions, these two bands diminished simultaneously and new absorption bands near $\lambda = 259$, 317 and 330 nm appeared (Figure 2 A). Similar observations were obtained for **P3** binding with Cu^{2+} ions in HEPES buffer (50 mM, pH 7.4): the absorption bands near $\lambda = 250$ and 281 nm of the metal-free peptoid diminished simultaneously upon addition of Cu^{2+} ions and new bands at $\lambda = 260$, 317 and 330 nm appeared (Figure S15). A metal-to-peptoid ratio plots, constructed from each titration, suggested 1:1 peptoid/Cu ratio (see inset in Figures 2 A, S14A) and the formation of the intramolecular Cu**P3** complex by simultaneous binding to both Terpy and HQ moieties.

To support these observations, 1 equiv of **P3** was mixed with 1.1 equiv of Cu^{2+} in un-buffered water (pH 7.0), and the solution was analyzed by HR-MS techniques. The obtained mass of 1395.55 matched the calculated mass of the intramolecular 1:1 Cu**P3** complex ($m/z = 1395.56$, Figures S17,18).

Next, Cu**P3** was characterised by CD spectroscopy. In un-buffered water (pH 7.0), the spectrum of a mixture solution containing 1 equiv of **P3** and 1 equiv of Cu^{2+} exhibits a double minima near 201 and 219 nm (typical for a helical Nspe peptoids, Figure S23A,B), and an exciton couplet CD peaks between 250 and 290 nm with maximum at 257 nm and minimum at 272 nm, crossing $\varepsilon = 0$ near 260 nm. This exciton couplet is similar to the previously reported CD spectrum of Cu**P1** complex, corresponding to the HQ π-π* transition (Figure S23C,D).[22b,26] Similar observations could be seen from the CD spectrum of Cu**P3** in HEPES buffer (10 mM, pH 7.4); a double-minima is obtained near 204 and 221 nm, along with exciton couplet peaks corresponding to the HQ π-π* transition appears with maximum at 256 nm and minimum at 268 nm. (Figure S23E,F).

Finally, the binding affinity of **P3** to Cu^{2+}, was estimated by a competition experiment with EDTA.[28] Thus, a mixture of **P3** and EDTA (17 μM each, in water, at pH 7.0) was titrated with Cu^{2+} followed by UV/Vis spectroscopy. The obtained data was analyzed according to a previously reported method.[28b] The dissociation constant K_D(Cu**P3**), represented by the slope between ([**P3**]$_{total}$/[Cu**P3**]−1) and ([EDTA]$_{total}$/[CuEDTA]−1), was found to be 3.7×10^{-16} M (Figure S24). From this we calculated that the association constant K_A(Cu**P3**) is 2.7×10^{15} M^{-1}.

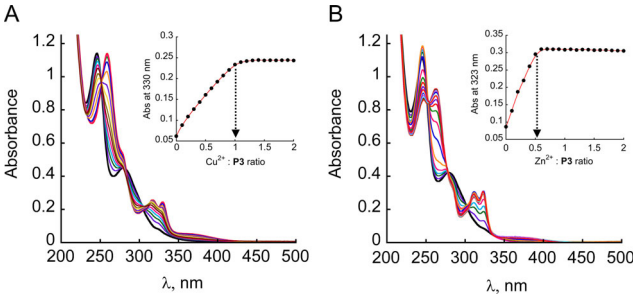

Figure 2. UV/Vis spectra and peptoid-to-metal ratio plot for the titration of **P3** A) with Cu^{2+} B) with Zn^{2+}. The peptoid (17 μM) in un-buffered water (pH 7.0) was titrated with 1 μL aliquots of a metal ion (5 mM in water) in multiple steps (black = free ligand, red = metal complex). pH after the titration was not significantly altered.

Binding of P3 to Zn^{2+} and Cu^{2+}

Titration of metal-free **P3** with Zn^{2+} ions (up to 0.5 equiv) in un-buffered water resulted in new absorption bands near $\lambda = 311$ and 323 nm (Figure 2 B), while almost no changes in the absorption near $\lambda = 246$ nm was recorded (Figure S14B), reflecting the exclusive binding of Zn^{2+} ions to the Terpy ligand. After addition of 0.5 equiv of Zn^{2+} ions the bands at $\lambda = 311$ and 323 nm became saturated, suggesting the formation of Zn(**P3**)$_2$ (Figure S14B). As the addition of Zn^{2+} continued, the band at $\lambda = 246$ nm decreased and the appearance of a new band at $\lambda = 263$ nm was recorded, indicating the binding of Zn^{2+} ions to the HQ ligands of **P3** (Figure S14B). Metal-to-peptoid ratio plots, constructed from this titration, suggested 1:2 Zn/peptoid ratio, which is consistent with the formation of intermolecular Zn(**P3**)$_2$ complex (Figure 2 B, inset) followed by the formation of the 2:2 Zn_2(**P3**)$_2$ (Figure S14B). ESI-MS analysis of this solution supported the formation of Zn_2(**P3**)$_2$ (Figures S19,20). In addition, ESI-MS analysis of a solution containing 1 equiv of **P3** that was treated with 0.5 equiv of Zn^{2+} in un-buffered water (pH 7.0), showed a mass of 1366.60, which matched the calculated half mass of the intermolecular 1:2 Zn(**P3**)$_2$ complex ($m/2z = 1366.28$, Figure S21,22). Titration of **P3** with Zn^{2+} in HEPES buffer showed similar results (Figure S16).

To support our observations and further characterize the formation of the intermolecular 1:2 Zn(**P3**)$_2$ and 2:2 Zn_2(**P3**)$_2$ complexes, the corresponding CD spectra were recorded. To 1 equiv of **P3**, either 0.5 equiv or 1 equiv of Zn^{2+} ions were added (Figure S23G,H and I,J, respectively). Similarly to Cu**P3**, both spectra exhibit double minima near 201, 204 and 219 nm. However, when only 0.5 equiv of Zn^{2+} were added, the CD spectrum did not show the exciton couplet CD peaks of the HQ π-π* transition, suggesting no binding between Zn^{2+} and the HQ ligands within **P3**. The exciton couplet CD peaks were obtained only when 1 equiv of Zn^{2+} ions was added to **P3** (with a maximum near 269 nm and minimum at 247 nm and 278 nm, crossing at $\varepsilon = 0$ twice, near 263 nm and 279 nm), suggesting binding of Zn^{2+} to HQ ligands only when the ratio between Zn^{2+} and **P3** is 1:1. Based on these observations we can suggest the following conclusions: (i) Zn(**P3**)$_2$ species, where the metal center is bound exclusively to Terpy ligands, while the HQ ligands of **P3** remain intact is formed first (up to 0.5 equiv of Zn^{2+} per peptoid), and (ii) in the presence of 1 equiv of Zn^{2+}, the first 0.5 equiv of Zn^{2+} binds two Terpy ligands intermolecularly, while the additional 0.5 equiv binds to the HQ ligands, producing 2:2 intermolecular Zn_2(**P3**)$_2$ species. Such a difference in Cu^{2+} versus Zn^{2+} binding to **P3** (concomitant binding to Terpy and HQ moiety for Cu^{2+} versus sequential for Zn^{2+}) may be in line with the higher Lewis acidity of Cu^{2+} that eases the deprotonation of the HQ moiety.

As the synaptic cleft contains excess of Zn^{2+} (compared to Cu^{2+}), we wished to understand whether **P3** could selectively bind Cu^{2+} when both metal ions are co-present. To explore the binding of Cu^{2+} in the presence of Zn^{2+} we conducted a few experiments in HEPES buffer, where we added both Cu^{2+} and Zn^{2+} ions, as a mixed solution (the mix approach) to **P3** and characterized the formed complexes by spectroscopic techniques. As a control, we have also characterized the binding to **P3** by adding one metal after the other (the step approach). Starting with the step approach, 1 equiv of metal-free **P3** in HEPES buffer (50 mM. pH 7.4) was treated with 0.5 equiv of Zn^{2+} and the changes were followed by UV/Vis (Figure 3A). The absorption band of Terpy at $\lambda = 281$ nm diminished and two new bands appeared simultaneously near $\lambda = 310$ and 323 nm, while the absorption band assigned to HQ showed only slight shift and no decrease in intensity, suggesting that the HQ ligands are not participating in the binding of Zn^{2+} ions, and that $Zn(\mathbf{P3})_2$ is formed exclusively in line with the titration experiment. Subsequent addition of 0.5 equiv of Cu^{2+} ions to this complex resulted in the formation of a new band at $\lambda = 261$ nm, indicating Cu^{2+} binding to the HQ ligands and suggesting the overall formation of $ZnCu(\mathbf{P3})_2$ (Figure 3A), in which Zn^{2+} is bound to two Terpy ligands and Cu^{2+} is bound to two HQ ligands (no change in the region near 320 nm corresponding to the Terpy moieties).

Continuing with a mix approach in the same reaction conditions, 1 equiv of metal-free **P3** was treated with a mixture containing 0.5 equiv of each Cu^{2+} and Zn^{2+}, and changes were also followed by UV/Vis. The spectrum of the obtained metallopeptoid was identical to the one obtained by the step approach (Figure 3A), which was assigned to the formation of $ZnCu(\mathbf{P3})_2$. As Zn^{2+} could bind to **P3** faster than Cu^{2+},[10a] we wanted to explore if Cu^{2+} can lead to the removal of Zn^{2+} from $Zn_2(\mathbf{P3})_2$. To this aim, we have conducted an experiment in HEPES buffer, in which excess Cu^{2+} ions (1 equiv instead of 0.5 equiv) was added to 1 equiv of **P3**, that was pre-incubated with 1 equiv of Zn^{2+} to form $Zn_2(\mathbf{P3})_2$. This experiment was followed by UV/Vis (Figure 3B). The obtained spectra exhibit a gradual shift in the absorbance bands near $\lambda = 264$, 312 and 323 nm, corresponding to the complex $Zn_2(\mathbf{P3})_2$, until these bands fully disappear and new bands near $\lambda = 260$, 317 and 330 nm appear, signifying the formation of the complex Cu**P3** (see Figure 2A above). At the working concentration of 20 μM, the metal exchange has a $t_{1/2}$ of about 170 s. The Cu, Zn complexes formation with **P3** was also probed by Electronic-Paramagnetic-Resonance (EPR, Figure S26). Under our sample preparation conditions (> 10 min), we detect only the Cu**P3** complex regardless of the presence of Zn. Overall, our results suggest that upon mixing molar equiv of **P3**, Cu^{2+} and Zn^{2+} ions in HEPES buffer, the complexes $ZnCu(\mathbf{P3})_2$ (not detected in the time scale of EPR sample preparation), and/or $Zn_2(\mathbf{P3})_2$, are formed first as kinetic products, and these will react selectively with the remaining Cu^{2+} to form Cu**P3** as a single thermodynamic product (Figure 3C). This conclusion indicated that **P3** is indeed selective to Cu^{2+} in the relevant conditions and concentrations, encouraging us to further explore the ability of **P3** to remove Cu^{2+} from Aβ and inhibit the production of ROS.

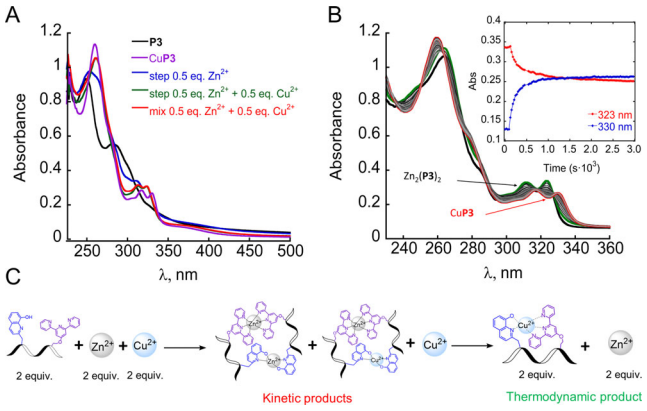

Figure 3. A) UV/Vis spectra describing Cu^{2+} binding to **P3** in the presence of Zn^{2+}. B) UV/Vis titration of $Zn(\mathbf{P3})_2$ complex with excess of Cu^{2+}. Inset: Kinetics of decrease in absorbance of $Zn(\mathbf{P3})_2$ (323 nm) and simultaneous increase in the absorbance of Cu**P3** (330 nm). Conditions: 20 μM of peptoid or peptoid complex in HEPES buffer (50 mM, pH 7.4) treated with 0.5 or 1 equiv of Cu^{2+}. C) A schematic representation of complexes formation from 2 equiv of **P3**, 2 equiv Cu^{2+} and 2 equiv Zn^{2+} using the mix approach, showing the formation of kinetic and thermodynamic products.

Reactive Oxygen Species Production

To probe ROS production, two approaches could be used. The first approach includes following the consumption of ascorbate by UV/Vis at 265 nm ($\varepsilon = 14\ 500\ M^{-1}\ cm^{-1}$), the reductant that fuels the formation of H_2O_2 or HO·.[29] In the second approach, the formation of HO· is followed by monitoring the fluorescence intensity of 7-hydroxy-coumarin-3-carboxylic acid (7-OH-CCA) dye that forms as a result of the reaction between HO· with coumarin-3-carboxylic acid (CCA).[30] The metal-ion binding sites of Aβ to Cu and Zn lie within residues 1–16,[31] therefore we have focused our study on the monomeric peptide $A\beta_{1-16}$ complex. In addition to it, the fibrillary forms of Aβ showed less activity than the monomeric peptide by one order of magnitude,[32] making the $A\beta_{1-16}$ peptide a good model for investigation.

Starting with the first approach, it was previously shown that, while a rapid consumption of ascorbate takes place in the presence of unbound copper, regardless of the co-presence of Zn^{2+} in the tested medium, when copper is bound to Aβ, this consumption slows down.[10,11a,29,32,33] We conducted ascorbate consumption experiments in order to evaluate the effect of **P3** on the production of ROS by Cu (in blue) or Cu-Aβ (in red) in the absence (Figure 4A–C) and in the presence (Figure 4D–F) of Zn^{2+}. In order to simulate all possible conditions for probing ROS production, three different ascorbate consumption experiments with three different starting points were performed: (1) starting from Cu^{2+} (Figure 4A, D) (2) starting from Cu^{+} (Figure 4B, E) and (3) starting from a mixture of Cu^{+} and Cu^{2+} (Figure 4C, F). In the first experiment, **P3** was added to Cu^{2+} or to Cu^{2+}-Aβ under aerobic conditions, followed by the addition of ascorbate. In

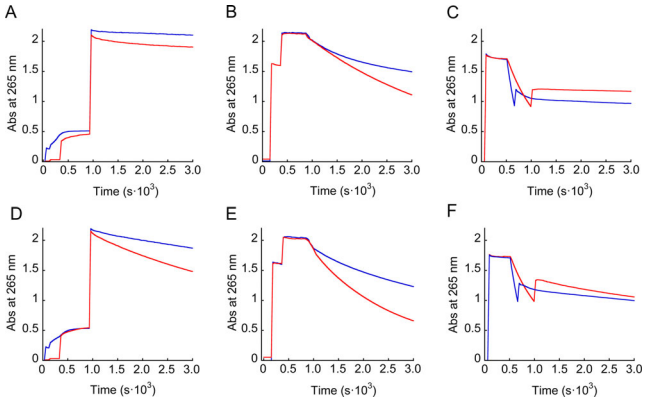

Figure 4. Kinetics of ascorbate consumption, followed by UV/Vis at 265 nm. A) Cu^{2+} + **P3** + Asc (blue), $A\beta_{1-16}$ + Cu^{2+} + **P3** + Asc (red). B) Cu^{2+} + Asc + **P3** + air (blue), $A\beta_{1-16}$ + Cu^{2+} + Asc + **P3** + air (red). C) Asc + Cu^{2+} + **P3** (blue), Asc + $A\beta_{1-16}$ + Cu^{2+} + **P3** (red). D) Cu^{2+} + Zn^{2+} + **P3** + Asc (blue), $A\beta_{1-16}$ + Cu^{2+} + Zn^{2+} + **P3** + Asc (red). E) Cu^{2+} + Zn^{2+} + Asc + **P3** + air (blue), $A\beta_{1-16}$ + Cu^{2+} + Zn^{2+} + Asc + **P3** + air (red). F) Asc + Cu^{2+} + Zn^{2+} + **P3** (blue), Asc + $A\beta_{1-16}$ + Cu^{2+} + Zn^{2+} + **P3** (red). The order of components in the text (A–F) represents the order of addition of the components in the cuvette. Conditions: [**P3**] = [$A\beta_{1-16}$] = [Zn^{2+}] = 10 μM, [Cu^{2+}] = 9 μM, [Asc] = 100 μM, [HEPES] = 50 mM, pH 7.4, with background subtraction of the signal at 800 nm.

the second experiment, Cu^{+} or Cu^{+}-Aβ are generated in situ by mixing these together with ascorbate under anaerobic conditions, followed by the addition of **P3** and then the sample was exposed to air to trigger the ascorbate consumption. In the last experiment, ascorbate was added to Cu^{2+} or Cu^{2+}-Aβ under aerobic conditions, followed by the addition of **P3**. Notably, in the third experiment, **P3** was added when the intensity was decreased from about 1.8 to about 0.9–1. As seen in Figure 4, each addition led to an increase in the intensity of the absorbance at 265 nm, which is attributed to the formation of the metal–peptoid complex (UV/Vis spectra of Cu and Zn complexes with **P3** are shown in Figure S25). After the addition of the last component, when the catalytic cycle should start, either no change in the intensity of the absorbance at 265 nm was observed, indicating no ascorbate consumption and thus no ROS production, or a sharp intensity decrease occurred, which suggests the consumption of ascorbate and formation of ROS.

Looking at Figure 4 A–C, we can see that **P3** is able to stop ascorbate consumption by both free Cu and Cu-Aβ complex only in experiments (1) and (3), while in experiment (2), when Cu^{2+} is added together with ascorbate in anaerobic conditions to form Cu^{+}, **P3** can only slow down the ascorbate consumption but not stop it (Figure 4 B), indicating that **P3** doesn't bind Cu^{+} under a redox inert form and/or can not extract Cu^{+} from Cu–Aβ complex. Interestingly, when **P3** was added in the presence of Zn^{2+} in all three experiments, the ascorbate consumption did not stop immediately but rather, only slowed down (Figure 4 D&F). These results indicate that the presence of Zn^{2+} ions limit the extraction of Cu^{2+} from Cu^{2+}-Aβ complex by **P3**. As a control, the same experiments in the same conditions were done in the absence of **P3** (Figure S33A–F), showing full ascorbate consumption.

Our conclusions from the UV/Vis experiments were further examined by measurements performed according to the second approach, in which the formation of HO· in the same experimental setups was followed by monitoring the fluorescence intensity of CCA. The results obtained from these fluorescence assays (Figure S34) matched perfectly those obtained from the ascorbate consumption experiments, supporting the ability of **P3** to prevent the ROS production caused by either free Cu ions or Cu-Aβ.

The limited ability of **P3** to stop the ROS production in the presence of Zn^{2+} ions is explained by our observation that $Zn(\mathbf{P3})_2$, $ZnCu(\mathbf{P3})_2$ complexes are formed first as the kinetic products, while the Cu**P3** is formed slower, as the thermodynamic product. Thus, **P3** should first bind mainly Zn^{2+}, leaving Cu-Aβ mostly intact, thus leading to ROS production, followed by the extraction of Cu^{2+} by **P3** complexes, eventually resulting in the arrest of ROS production. It should be noted that the formation of the Aβ-Cu/Zn-**P3** ternary species, where Cu remains partially bound to Aβ, and therefore continues to participate in the redox cycle, could occur in parallel to described above events. Formation of ternary species has been reported to occur at physiological conditions,[3a,b,34] and therefore should be excluded from the possible pathway of action of **P3**, and full extraction of Cu from Cu/CuZn-Aβ complex should be proven first. To support full extraction of Cu from CuAβ/CuZnAβ complex by **P3**, CD and EPR experiments were performed.

Cu^{2+} Extraction from Cu–Aβ Complex in the Absence and Presence of Zn^{2+}

After having shown the thermodynamic selectivity of **P3** for Cu^{2+} (compared to Zn^{2+}) and the likely Zn^{2+}-induced slow-down of ROS lessening by **P3**, we investigated by CD and EPR whether **P3** has a higher selectivity than Aβ, a prerequisite to remove Cu^{2+} from Aβ in presence of Zn^{2+}.[3a,10] The CD spectrum of free $A\beta_{1-16}$ in HEPES buffer (10 mM, pH 7.4) exhibits two bands with a minimum near 201 nm and a maximum near 223 nm (Figure S36A), indicating the presence of the polyproline type II (PPII) helical structure conformation, as previously reported.[35] The addition of 1 equiv of Cu^{2+} to the solution resulted in an intensity decrease of both bands (Figure S36B), indicating the weakening of the helical conformation of $A\beta_{1-16}$ resulted from the partial change of it to β-sheet upon binding to Cu^{2+} ions.[35] In contrast, addition of 1 equiv of Zn^{2+} to 1 equiv of $A\beta_{1-16}$ showed a slight increase in the positive band near 223 nm (Figure S36C), suggesting that ZnAβ species maintain the initial conformational preference, and that the Zn^{2+} ions rather stabilize the overall conformation of $A\beta_{1-16}$ at the chosen conditions. Interestingly, when both Cu^{2+} and Zn^{2+} were added to a solution of 1 equiv of $A\beta_{1-16}$, the obtained spectrum resembled the spectrum of CuAβ (Figure S36D), suggesting that Cu^{2+} binds to the same binding site in both experiments and that Zn^{2+} ions do not interfere strongly with the binding to $A\beta_{1-16}$, in line with previous report.[29] The changes in the positive band of $A\beta_{1-16}$ upon its binding to the metal ions are summarized in Figure S36.

As the addition of Cu^{2+} to $A\beta_{1-16}$ leads to a decrease in the absorbance band near 200 nm, extraction of Cu^{2+} by **P3** should lead to an increase in intensity of this band. However, **P3** has an intense minimum near 200 nm, thus it is difficult to make a conclusion regarding the extraction of Cu^{2+} based on this band. In contrast, **P3**, Zn(**P3**)$_2$, $A\beta_{1-16}$, CuAβ, ZnAβ and CuZnAβ do not absorb at the 250–300 nm range (see SI), while Cu**P3** and Zn_2(**P3**)$_2$ exhibit band(s) in this range with a minimum near 270 nm (Cu**P3**, Figure 5 A and S23D,F) or with a maximum near 270 nm and a minimum near 280 nm (Zn_2(**P3**)$_2$, Figure 5 B and 23J). Therefore, obtaining a single minimum band near 270 nm in competition experiments between $A\beta_{1-16}$ and **P3** for Cu^{2+} binding will be a clear indication for the exclusive formation of Cu**P3.**

To probe this point, extraction of Cu from CuAβ complex by **P3** in the absence and presence of Zn was studied by CD spectroscopy. First, mixtures of 1 equiv of $A\beta_{1-16}$ and Cu^{2+} or Cu^{2+}/Zn^{2+} mixture (0.9 equiv and 0.9:1 equiv, respectively) in HEPES buffer (10 mM, pH 7.4) were allowed to react for 5 min and then their CD spectra were recorded and compared to the CD of **P3** in the same conditions (Figure 5 C,D, black curves). Next, 1 equiv of **P3** were added to the mixtures and the solutions were incubated for 24 hours, before their CD spectra were measured and compared to the spectrum of **P3** with Cu^{2+} (Figure 5 C,D blue curves, and S37). These spectra show a single band with a minimum between 270–280 nm, resembling the spectrum of Cu**P3**, which suggests the successful extraction of Cu from CuAβ/CuZnAβ complex.

To further probe the ability of **P3** to remove Cu^{2+} from $A\beta_{1-16}$, EPR is the method of choice.[10a] Figure 6 shows the monitoring of $A\beta_{1-16}$-bound Cu^{2+} extraction by **P3** in absence

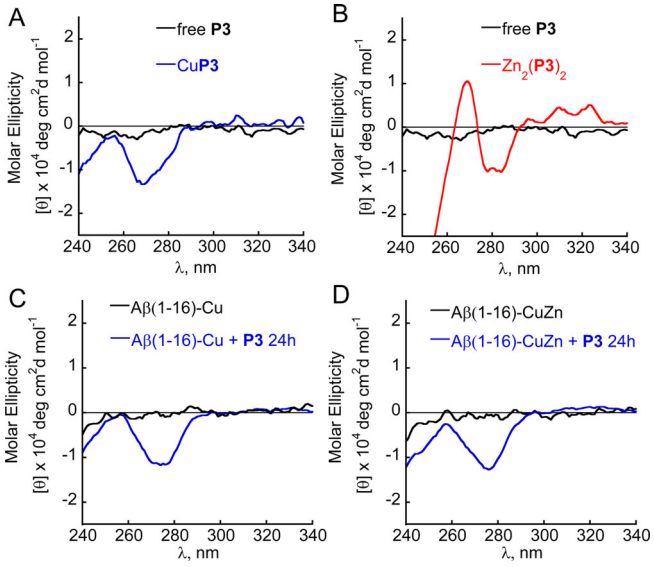

Figure 5. CD studies for Cu^{2+} extraction from Cu-Aβ complex in the the absence and presence of Zn^{2+}. CD spectrum of the near UV range for A) free **P3** (black) and Cu^{2+} + **P3** (blue), B) free **P3** (black) and Zn^{2+} + **P3** (red), C) $A\beta_{1-16}$ + Cu^{2+} (black) and $A\beta_{1-16}$ + Cu^{2+} + **P3** (blue), D) $A\beta_{1-16}$ + Cu^{2+} + Zn^{2+} (black) and $A\beta_{1-16}$ + Cu^{2+} + Zn^{2+} + **P3** (blue). The order of components in the text (A–D) represents the order of addition of the components in the cuvette. Conditions: [**P3**] = [$A\beta_{1-16}$] = [Zn^{2+}] = 100 μM, [Cu^{2+}] = 90 μM, [HEPES] = 10 mM, pH 7.4.

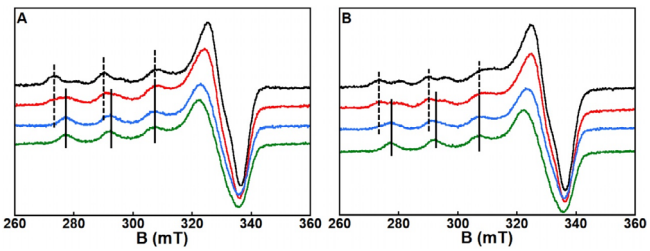

Figure 6. EPR spectra of A) Cu^{2+} + **P3** (green), $A\beta_{1-16}$ + Cu^{2+} (black), $A\beta_{1-16}$ + Cu^{2+} + **P3**—EPR tube frozen asap (red) and $A\beta_{1-16}$ + Cu^{2+} + **P3**—EPR tube frozen after two hours (blue). B) Cu^{2+} + **P3** (green), $A\beta_{1-16}$ + Cu^{2+} + Zn^{2+} (black),[a] $A\beta_{1-16}$ + Cu^{2+} + Zn^{2+} + **P3**—EPR tube frozen asap (red), $A\beta_{1-16}$ + Cu^{2+} + Zn^{2+} + **P3**—EPR tube frozen after two hours (blue). [a] Note that the difference in the EPR signature of Cu- $A\beta_{1-16}$ with or without Zn is due to the co-binding of Zn to the Aβ peptide and has been documented before.[29] Conditions: [**P3**] = [$A\beta_{1-16}$] = [Zn^{2+}] = 200 μM, [Cu^{2+}] = 180 μM, [HEPES] = 50 mM, pH 7.4. Recording conditions: T = 120 K, ν = 9.5 GHz, modulation amplitude = 5 G, microwave power: 20 mW.

of Zn, with the sample frozen as soon as possible after addition of **P3** (panel A, red line) and after 2 hours (panel A, blue line). In panel B, the same experiment is performed on CuZnAβ complex. In green lines, are the EPR signature of Cu-**P3**, in black lines that of Cu^{2+}-$A\beta_{1-16}$ or CuZnAβ in presence of one equiv of Zn and in red and blue lines the resulting species after addition of **P3**. Cu-**P3** is characterized by the following ^{65}Cu-EPR parameters: $g_{\parallel} = 2.26$ $A_{\parallel} = 160 \times 10^{-4}$ cm^{-1} and $g_{\perp} = 2.06$, while the signature of Cu-$A\beta_{1-16}$ is identical as that previously reported with two species co-existing at pH 7.4.[31,36] Hyperfine lines of Cu-**P3** and Cu-$A\beta_{1-16}$ are shown in plain and dotted lines, respectively. In absence of Zn, and upon addition of **P3**, the EPR signature corresponds to a mixture of Cu-$A\beta_{1-16}$ and Cu-**P3** species in about a 1:1 ratio (panel A, red line). After two hours (panel A, blue line), the EPR signature of the mixture is superimposable to that of Cu-**P3**. In presence of Zn, the spectrum recorded immediately after **P3** addition is similar to the one of Cu-Aβ (panel B, red line) while after two hours, the signature of Cu-**P3** is detected (panel B, blue line). The EPR experiment perfectly demonstrates that (i) Cu is removed from $A\beta_{1-16}$ regardless of the presence of Zn and (ii) in presence of Zn, the Cu extraction takes more time. In other words, the thermodynamic Cu over Zn selectivity of **P3** is fully appropriate,[10b,3b] while Zn has a kinetic effect on the Cu^{2+} extraction from $A\beta_{1-16}$.

Overall, the CD and EPR experiments exclude the possible formation of Aβ-Cu/Zn-**P3** ternary species in significant amount. To further explore whether the limited ability of **P3** for immediate arrest of ROS production in the presence of Zn^{2+} is indeed related to the differences in kinetics of Cu^{2+} and Zn^{2+} coordination to **P3**, we set to evaluate the rates of Cu^{2+} and Zn^{2+} binding to **P3** in the relevant reaction conditions.

Kinetic Study

To evaluate to which of the metal ions, Cu^{2+} or Zn^{2+}, **P3** coordinates first, we measured the rates of Cu^{2+} and Zn^{2+} binding to **P3** in the presence of Aβ peptide. Thus, 1 equiv of **P3** was added to a buffered solution of quasi-stoichiometric amount of each metal ion (0.9 equiv of Cu^{2+} and/or 1 equiv of Zn^{2+}, respectively) and 1 equiv of Aβ. The Aβ and metal ions were allowed to react for 500 s to ensure complex formation prior to the addition of 1 equiv of **P3**. The reactions were followed by UV/Vis spectroscopy and the results are depicted in Figure 7 A–D. In the case of single metal–peptoid complex formation, we can see that while Cu^{2+} binds faster than Zn^{2+} to the HQ binding site of **P3** (Figure 7 A, green versus black, respectively (formation of complex); and purple versus blue, respectively (consumption of **P3**), both Cu^{2+} and Zn^{2+} bind at similar rate to the Terpy site (Figure 7 B, blue and red curves, respectively). In the presence of the mixture of both Cu^{2+} and Zn^{2+} metal ions several observations can be made: (i) the reactions are faster as expected due to double concentration of the metal ions; (ii) the decrease in the curves showed in Figure 7 D indicates that the Terpy binding site of **P3** initially binds Zn^{2+}, followed by binding to Cu^{2+} (see also Figure S40, where the arrow indicates a shift of metal-complex absorption band from 311–323 nm for Zn**P3** species towards 317–330 nm, that corresponds to Cu**P3** species); (iii) the slight decrease in the curves showed in Figure 7 C (green and black curves) can suggest the simultaneous formation of several species; the overall decrease (Figure 7 C) indicates that like the Terpy site, the HQ site of **P3** initially binds Zn^{2+}, followed by the binding to Cu^{2+} (see also Figure S40, where the arrow in spectra indicates shift of metal-complex absorption band from 264 nm for Zn**P3** species towards 260 nm, that corresponds to Cu**P3** species).

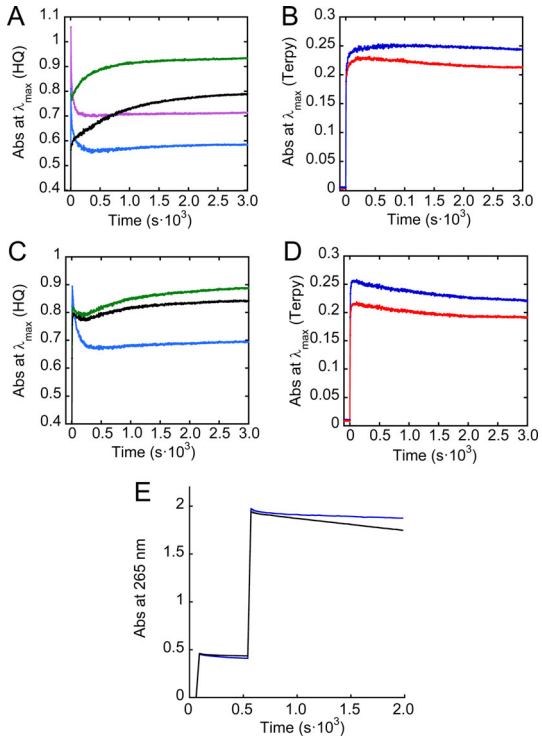

Figure 7. Kinetics of Cu or Zn extraction by **P3** from CuAβ or ZnAβ at A) HQ region: Cu^{2+}-$Aβ_{1–16}$ + **P3** at 250 nm (purple) and at 260 nm (green), and Zn^{2+}-$Aβ_{1–16}$ + **P3** at 250 nm (light blue) and at 264 nm (black); B) Terpy region: Cu^{2+}-$Aβ_{1–16}$ + **P3** at 329 nm (blue) and Zn^{2+}-$Aβ_{1–16}$ + **P3** at 323 nm (red). Kinetics of Cu,Zn competition extraction by **P3** from the Cu,Zn-Aβ complex at C) HQ region: Cu^{2+},Zn^{2+}-$Aβ_{1–16}$ + **P3** at 250 nm (light blue), at 260 nm (green) and at 264 nm (black) or D) Terpy region: Cu^{2+},Zn^{2+}-$Aβ_{1–16}$ + **P3** at 329 nm (blue) or at 323 nm (red) Conditions: [**P3**] = [$Aβ_{1–16}$] = [Zn^{2+}] = 20 μM, [Cu^{2+}] = 18 μM [HEPES] = 50 mM, pH 7.4, with background subtraction of the signal at 800 nm. Additions of **P3** were performed at t = 0 s. E) Ascorbate consumption in pre-incubated solution of Cu^{2+}-$Aβ_{1–16}$-**P3** (blue curve) or $Cu^{2+}Zn^{2+}$-$Aβ_{1–16}$-**P3** (black curve) for 24 hours. Ascorbate was added at t = 541 s to ensure that the absorbance intensity of the formed species is stabilized. Conditions: [**P3**] = [$Aβ_{1–16}$] = [Zn^{2+}] = 10 μM, [Cu^{2+}] = 9 μM, [Asc] = 100 μM, [HEPES] = 50 mM, pH 7.4, with background subtraction of the signal at 800 nm.

Overall, the kinetic data demonstrates that in the presence of Zn^{2+} the extraction of Cu^{2+} ions by **P3** is slowed down by the formation of Zn**P3** complexes as kinetic products, and this hinders the immediate inhibition of ROS production. However, our data shows that **P3** can extract Cu^{2+} ions in the presence of Zn^{2+}, which leads to the formation of Cu**P3** as the thermodynamic product and results in some inhibition of ROS production also in the presence of Zn^{2+}. As the full extraction of Cu^{2+} by **P3** is a thermodynamic process, we wanted to see if we could increase ROS inhibition using this result. To this aim, Cu^{2+} and Zn^{2+} ions were added simultaneously to Aβ to form the complexes Cu-Aβ or CuZn-Aβ, (as indicated by UV/Vis, Figure S41A), followed by the addition of **P3**, and the solution was incubated for 24 hours. After 24 hours, the UV/Vis spectrum of this solution was measured (Figure S41B), and the obtained spectrum in the presence of Zn^{2+} indicated the formation of the mixture of species. Thereafter ascorbate was added, and the spectrum showed almost no consumption −12 % consumption (Figure 7 E) vs. 32 % consumption in 25 min for the same experiment, performed without pre-incubation (Figure 4 D). These results, together with the data presented in Figure 4 D–F, support the extraction Cu^{2+} from CuZn-Aβ by **P3** to form Cu**P3** via a thermodynamic process, and allow for almost full inhibition of ROS production also in the presence of Zn^{2+} ions.

To correlate the amount of **P3**-bound Cu^{2+} and Zn^{2+} with the amount of ascorbate that is consumed during the reaction, we constructed a calibration curve by following the addition of 1 equiv of **P3** to a set of Cu^{2+} and Zn^{2+} mixtures in different equiv ratios, via UV/Vis (Figure S42). The recorded spectrum of each mixture was compared to the corresponding spectrum obtained from the ascorbate consumption experiments. The results (Table S5,6 and Figure S43) suggest the following: (i) without pre-incubation, about 50–70 % of Cu^{2+} and 30–50 % of Zn^{2+} are bound to the **P3**, which is in agreement with the amount of ascorbate consumption (about 32 %), (ii) with pre-incubation, about 80–90 % of Cu^{2+} and no more than 10–20 % of Zn^{2+} are bound to the **P3**, and this also correlates with the amount of ascorbate consumption in this case (about 12 %).

Our observations support our hypothesis as depicted in Scheme 2. In the absence of Zn^{2+}, the extraction of Cu^{2+} from Aβ is immediate, and so is ROS inhibition, which is fully

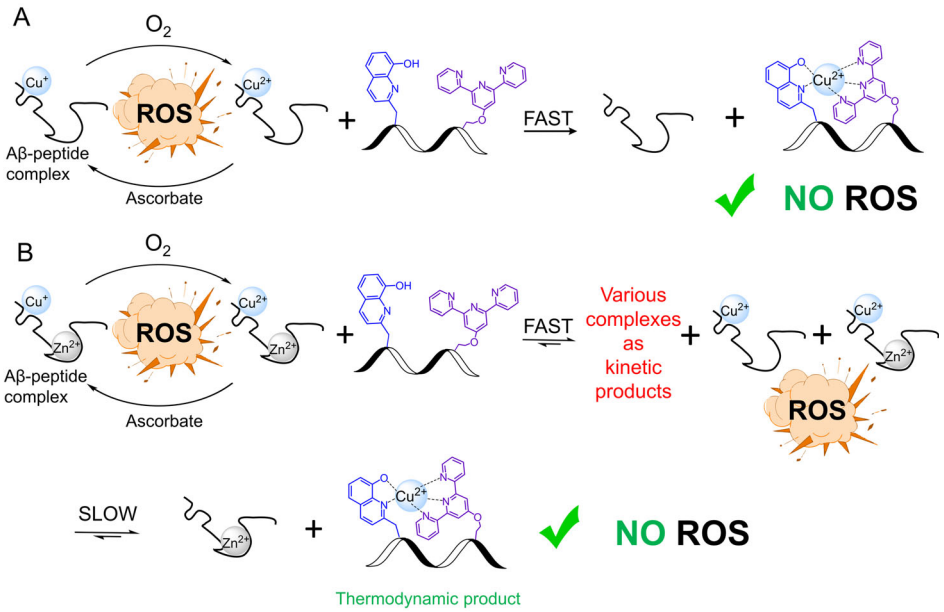

Scheme 2. Schematic summary of Cu chelation and ROS production/inhibition by the peptoid **P3** in the presence of ascorbate and Aβ and in the absence (A) or presence (B) of Zn^{2+}.

achieved (Scheme 2A), while in the presence of Zn^{2+} the extraction of Cu^{2+} ions by **P3** is slower than the extraction of Zn^{2+} and therefore various complexes are formed as kinetic products, hindering the immediate inhibition of ROS production (Scheme 2B).

Conclusion

Herein we showed that the incorporation of one piperazine group at the C-terminus of a water-insoluble hydrophobic helical peptoid chelator with high selectivity to Cu^{2+} resulted in the water-soluble peptoid chelator **P3**. We demonstrated that the selectivity of **P3** to Cu^{2+}, in the presence of excess of other metal ions, including Zn, is preserved also in water. Selectivity to Cu in the presence of Zn is extremely important in the context of AD, because the ionic pool of the synaptic cleft, where Aβ aggregation and ROS production take place, contains excess of Zn, which can potentially hinder Cu binding by an external chelator due to possible similarities in the binding preferences of these two metal ions. However, we show that **P3** binds Cu^{2+} and Zn^{2+} differently: Cu^{2+} binds HQ and Terpy simultaneously, leading exclusively to the 1:1 metal/peptoid intramolecular Cu**P3** complex, while Zn^{2+} binds first two Terpy ligands from two peptoids in a 1:2 metal/peptoid ratio, forming the intermolecular $Zn(\mathbf{P3})_2$ complex, followed by the binding of additional equiv of Zn or Cu^{2+} that are present in solution, forming the complexes $Zn_2(\mathbf{P3})_2$ or $ZnCu(\mathbf{P3})_2$, respectively.

Despite the fast formation of Zn complexes being kinetically favored products, as illustrated from the mixture and step approach and kinetic studies, Cu^{2+} ions can replace Zn from these complexes, resulting in the formation of Cu**P3** as an exclusive thermodynamic product. Furthermore, we show here for the first time, that the selectivity of this water-soluble peptoid chelator, **P3**, to Cu^{2+} can be used in the context of AD: **P3** can successfully extract Cu^{2+} from the CuAβ-complex even in the presence of Zn ions, to form the thermodynamically stable complex Cu**P3**, and by this enables the inhibition of ROS production in a reducing environment at physiological pH (Scheme 2), as confirmed by both ascorbate consumption experiments and CCA Fluorescence assays. These unique abilities of **P3**, combined with the advantages of peptoids as therapeutics including their high proteolytic resistance, high membrane permeability and tolerance towards high salts concentrations, make **P3** an excellent chelator compared to the other peptidomimetic ligands known as drug candidates in a context of AD.

Further studies will focus on possible modifications of the **P3** sequence to allow full arrest of ROS production caused by CuAβ-complex, in physiological conditions and in biological systems. In addition, the effect of **P3**, as well as similar peptoid chelators, on the aggregation of Aβ peptides, associated with high toxicity, will be further evaluated.

Acknowledgements

This work was supported by the Israel Science Foundation (ISF) grant number 395/16 awarded to G.M. and by the European Council of Science (ERC) grant StG638712 "aLzINK" awarded to C.H. The authors thank Mrs. Larisa Panz for her assistance with MS measurements. A.B. thanks the Schulich Foundation for her PhD fellowship.

Conflict of Interest

The authors declare no conflict of interest.

Keywords: Alzheimer's disease · amyloids · Cu chelators · peptides · peptoids · Zn

[1] E. I. Solomon, D. E. Heppner, E. M. Johnston, J. W. Ginsbach, J. Cirera, M. Qayyum, M. T. Kieber-Emmons, C. H. Kjaergaard, R. G. Hadt, L. Tian, *Chem. Rev.* **2014**, *114*, 3659 – 3853.

[2] A. I. Bush, *Curr. Opin. Chem. Biol.* **2000**, *4*, 184.

[3] a) M. G. Savelieff, G. Nam, J. Kang, H. J. Lee, M. Lee, M. H. Lim, *Chem. Rev.* **2019**, *119*, 1221 – 1322; b) C. Esmieu, D. Guettas, A. Conte-daban, L. Sabater, P. Faller, C. Hureau, *Inorg. Chem.* **2019**, *58*, 13509 – 13527; c) C. Cheignon, M. Tomas, D. Bonnefont-Rousselot, P. Faller, C. Hureau, F. Collin, *Redox Biol.* **2018**, *14*, 450 – 464; d) E. Atrián-Blasco, P. Gonzalez, A. Santoro, B. Alies, P. Faller, C. Hureau, *Coord. Chem. Rev.* **2018**, *371*, 38 – 55.

[4] a) P. Faller, C. Hureau, O. Berthoumieu, *Inorg. Chem.* **2013**, *52*, 12193 – 12206; b) A. Tiiman, P. Palumaa, V. Tõugu, *Neurochem. Int.* **2013**, *62*, 367 – 378.

[5] a) S. Ayton, P. Lei, A. I. Bush, *Neurotherapeutics* **2015**, *12*, 109 – 120; b) V. Chiurchiù, A. Orlacchio, M. Maccarrone, *Oxid. Med. Cell. Longevity* **2016**, *2016*, 7909380; c) N. Xia, L. Liu, *Mini-Rev. Med. Chem.* **2014**, *14*, 271 – 281; d) P. J. Crouch, K. J. Barnham, *Acc. Chem. Res.* **2012**, *45*, 1604 – 1611; e) K. J. Barnham, A. I. Bush, *Chem. Soc. Rev.* **2014**, *43*, 6727 – 6749; f) A. Robert, Y. Liu, M. Nguyen, B. Meunier, *Acc. Chem. Res.* **2015**, *48*, 1332 – 1339; g) C. Hureau, P. Faller, *Biochimie* **2009**, *91*, 1212 – 1217.

[6] a) J. Kardos, I. Kovfics, F. Hajs, M. Kfilmfin, M. Simonyi, *Neurosci. Lett.* **1989**, *103*, 139 – 144; b) D. E. Hartter, A. Barnea, *Synapse* **1988**, *2*, 412 – 415; c) C. J. Frederickson, *Int. Rev. Neurobiol.* **1989**, *31*, 145 – 238.

[7] a) I. Zawisza, M. Rozga, W. Bal, *Coord. Chem. Rev.* **2012**, *256*, 2297 – 2307; b) S. Noël, S. Bustos, S. Sayen, E. Guillon, P. Faller, C. Hureau, *Metallomics* **2014**, *6*, 1220 – 1222.

[8] B. Alies, E. Renaglia, M. Rozga, W. Bal, P. Faller, C. Hureau, *Anal. Chem.* **2013**, *85*, 1501 – 1508.

[9] C. Hureau in *Encyclopedia of Inorganic and Bioinorganic Chemistry* (Eds.: R. A. Scott), Wiley, Hoboken, **2018**, pp. 1 – 14.

[10] a) A. Conte-Daban, A. Day, P. Faller, C. Hureau, *Dalton Trans.* **2016**, *45*, 15671 – 15678; b) E. Atrián-Blasco, A. Conte-Daban, C. Hureau, *Dalton Trans.* **2017**, *46*, 12750 – 12759.

[11] a) P. Faller, C. Hureau, *Dalton Trans.* **2009**, 1080 – 1094; b) M. A. Santos, K. Chand, S. Chaves, *Coord. Chem. Rev.* **2016**, *327 – 328*, 287 – 303.

[12] S. C. Drew, *Front. Neurosci.* **2017**, *11*, 317.

[13] R. Squitti, C. Salustri, M. Rongioletti, M. Siotto, *Front. Neurol.* **2017**, *8*, 503.

[14] P. Faller, C. Hureau, *Chem. Eur. J.* **2012**, *18*, 15889 – 15889.

[15] a) J. L. Arbiser, S. K. Kraeft, R. van Leeuwen, S. J. Hurwitz, M. Selig, G. R. Dickersin, A. Flint, H. R. Byers, L. B. Chen, *Mol. Med.* **1998**, *4*, 665 – 670; b) M. K. Lawson, M. Valko, M. T. D. Cronin, K. Jomová, *Curr. Pharmacol. Rep.* **2016**, *2*, 271 – 280.

[16] a) Y. Kwon, T. Kodadek, *J. Am. Chem. Soc.* **2007**, *129*, 1508 – 1509; b) J. Schwochert, R. Turner, M. Thang, R. F. Berkeley, A. R. Ponkey, K. M. Rodriguez, S. S. F. Leung, B. Khunte, G. Goetz, C. Limberakis, A. S. Kalgutkar, H. Eng, M. J. Shapiro, A. M. Mathiowetz, D. A. Price, S. Liras, M. P. Jacobson, R. Scott Lokey, *Org. Lett.* **2015**, *17*, 2928 – 2931; c) A. Furukawa, C. E. Townsend, J. Schwochert, C. R. Pye, M. A. Bednarek, R. Scott Lokey, *J. Med. Chem.* **2016**, *59*, 9503 – 9512; d) N. C. Tan, P. Yu, Y. U. Kwon, T. Kodadek, *Bioorg. Med. Chem.* **2008**, *16*, 5853 – 5861.

[17] J. Seo, B.-C. Lee, R. N. Zuckermann in *Comprehensive Biomaterials*, *Vol. 2* (Eds.: P. Ducheyne, K. E. Healy, D. W. Hutmacher, D. W. Grainger, C. J. Kirkpatrick), Elsevier, Amsterdam, **2011**, pp. 53 – 76.

[18] R. N. Zuckermann, J. M. Kerr, W. H. Moosf, S. B. H. Kent, *J. Am. Chem. Soc.* **1992**, *114*, 10646 – 10647.

[19] R. J. Simon, R. S. Kania, R. N. Zuckermann, V. D. Huebner, D. A. Jewell, S. Banville, S. Ng, L. Wang, S. Rosenberg, C. K. Marlowe, *Proc. Natl. Acad. Sci. USA* **1992**, *89*, 9367 – 9371.

[20] a) K. Kirshenbaum, A. E. Barron, R. A. Goldsmith, P. Armand, E. K. Bradley, K. T. V. Truong, K. A. Dill, F. E. Cohen, R. N. Zuckermann, *Proc. Natl. Acad. Sci. USA* **1998**, *95*, 4303 – 4308; b) C. W. Wu, K. Kirshenbaum, T. J. Sanborn, J. A. Patch, K. Huang, K. A. Dill, R. N. Zuckermann, A. E. Barron, *J. Am. Chem. Soc.* **2003**, *125*, 13525 – 13530; c) J. R. Stringer, J. A. Crapster, I. A. Guzei, H. E. Blackwell, *J. Am. Chem. Soc.* **2011**, *133*, 15559 – 15567; d) J. A. Crapster, I. A. Guzei, H. E. Blackwell, *Angew. Chem. Int. Ed.* **2013**, *52*, 5079 – 5084; *Angew. Chem.* **2013**, *125*, 5183 – 5188; e) O. Roy, G. Dumonteil, S. Faure, L. Jouffret, A. Kriznik, C. Taillefumier, *J. Am. Chem. Soc.* **2017**, *139*, 13533 – 13540.

[21] a) J. T. Nguyen, C. W. Turck, F. E. Cohen, R. N. Zuckermann, W. A. Lim, *Science* **1998**, *282*, 2088 – 2092; b) T. Hara, S. R. Durell, M. C. Myers, D. H. Appella, *J. Am. Chem. Soc.* **2006**, *128*, 1995 – 2004; c) D. G. Udugamasooriya, S. P. Dineen, R. A. Brekken, T. A. Kodadek, *J. Am. Chem. Soc.* **2008**, *130*, 5744 – 5752.

[22] a) B. C. Lee, T. K. Chu, K. A. Dill, R. N. Zuckermann, *J. Am. Chem. Soc.* **2008**, *130*, 8847 – 8855; b) G. Maayan, M. D. Ward, K. Kirshenbaum, *Chem. Commun.* **2009**, 56 – 58; c) A. D'Amato, P. Ghosh, C. Costabile, G. Della Sala, I. Izzo, G. Maayan, F. De Riccardis, *Dalton Trans.* **2020**, *49*, 6020 – 6029; d) P. Ghosh, G. Maayan, *Chem. Sci.* **2020**, *11*, 10127 – 10134; e) P. Ghosh, G. Maayan, *Chem. Eur. J.* **2021**, *27*, 1383.

[23] a) G. Maayan, M. D. Ward, K. Kirshenbaum, *Proc. Natl. Acad. Sci. USA* **2009**, *106*, 13679 – 13684; b) G. Della Sala, B. Nardone, F. De Riccardis, I. Izzo, *Org. Biomol. Chem.* **2013**, *11*, 726 – 731; c) R. Schettini, B. Nardone, F. De Riccardis, G. Della Sala, I. Izzo, *Eur. J. Org. Chem.* **2014**, 7793 – 7797; d) K. J. Prathap, G. Maayan, *Chem. Commun.* **2015**, *51*, 11096 – 11099; e) R. Schettini, F. De Riccardis, G. Della Sala, I. Izzo, *J. Org. Chem.* **2016**, *81*, 2494 – 2505; f) C. M. Darapaneni, P. Ghosh, T. Ghosh, G. Maayan, *Chem. Eur. J.* **2020**, *26*, 9573 – 9579; g) T. Ghosh, P. Ghosh, G. Maayan, *ACS Catal.* **2018**, *8*, 10631 – 11064.

[24] S. M. Miller, R. J. Simon, S. Ng, R. N. Zuckermann, J. M. Kerr, W. H. Moos, *Drug Dev. Res.* **1995**, *35*, 20 – 32.

[25] a) Y. Luo, S. Vali, S. Sun, X. Chen, X. Liang, T. Drozhzhina, E. Popugaeva, I. Bezprozvanny, *ACS Chem. Neurosci.* **2013**, *4*, 952 – 962; b) J. P. Turner, T. Lutz-Rechtin, K. A. Moore, L. Rogers, O. Bhave, M. A. Moss, S. L. Servoss, *ACS Chem. Neurosci.* **2014**, *5*, 552 – 558; c) K. Pradhan, G. Das, V. Gupta, P. Mondal, S. Barman, J. Khan, S. Ghosh, *ACS Chem. Neurosci.* **2019**, *10*, 1355 – 1368.

[26] M. Baskin, G. Maayan, *Chem. Sci.* **2016**, *7*, 2809 – 2820.

[27] C. M. Darapaneni, P. J. Kaniraj, G. Maayan, *Org. Biomol. Chem.* **2018**, *16*, 1480 – 1488.

[28] a) Z. Xiao, A. G. Wedd, *Nat. Prod. Rep.* **2010**, *27*, 768 – 789; b) L. Zhang, M. Koay, M. J. Maher, Z. Xiao, A. G. Wedd, *J. Am. Chem. Soc.* **2006**, *128*, 5834 – 5850.

[29] B. Alies, I. Sasaki, O. Proux, S. Sayen, E. Guillon, P. Faller, C. Hureau, *Chem. Commun.* **2013**, *49*, 1214 – 1216.

[30] S. Chassaing, F. Collin, P. Dorlet, J. Gout, C. Hureau, P. Faller, *Curr. Top. Med. Chem.* **2012**, *12*, 2573 – 2595.

[31] C. Hureau, *Coord. Chem. Rev.* **2012**, *256*, 2164 – 2174.

[32] J. T. Pedersen, S. W. Chen, C. B. Borg, S. Ness, J. M. Bahl, N. H. H. Heegaard, C. M. Dobson, L. Hemmingsen, N. Cremades, K. Teilum, *J. Am. Chem. Soc.* **2016**, *138*, 3966 – 3969.

[33] a) M. Miller, Q. W. Tejas, P. Telivala, R. J. Smith, A. Lanzirotti, J. Miklossy, *J. Struct. Biol.* **2006**, *155*, 30 – 37; b) A. Conte-Daban, B. Boff, A. Candido Matias, C. N. M. Aparicio, C. Gateau, C.

Lebrun, G. Cerchiaro, I. Kieffer, S. Sayen, E. Guillon, P. Delangle, C. Hureau, *Chem. Eur. J.* **2017**, *23*, 17078.
[34] V. B. Kenche, I. Zawisza, C. L. Masters, W. Bal, K. J. Barnham, S. C. Drew, *Inorg. Chem.* **2013**, *52*, 4303 – 4318.
[35] D. Yugay, D. P. Goronzy, L. M. Kawakami, S. A. Claridge, T.-B. Song, Z. Yan, Y.-H. Xie, J. Gilles, Y. Yang, P. S. Weiss, *Nano Lett.* **2016**, *16*, 6282 – 6289.
[36] S. C. Drew, K. J. Barnham, *Acc. Chem. Res.* **2011**, *44*, 1146 – 1155.

Manuscript received: July 21, 2021
Revised manuscript received: September 1, 2021
Accepted manuscript online: September 12, 2021
Version of record online: ■■ ■■, ■■■■

Research Articles

Amyloid β-peptides

A. E. Behar, L. Sabater, M. Baskin, C. Hureau,* G. Maayan* — ■■■■–■■■■

A Water-Soluble Peptoid Chelator that Can Remove Cu^{2+} from Amyloid-β Peptides and Stop the Formation of Reactive Oxygen Species Associated with Alzheimer's Disease

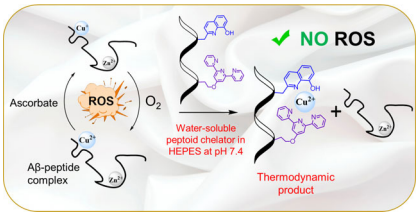

Cu-chelation from amyloid-β (Aβ) peptide complexes is a known approach towards the development of therapeutics for Alzheimer's disease (AD), the most common form of dementia. Herein we describe a water-soluble peptidomimetic chelator that removes Cu from Cu–Aβ in the presence of Zn, forming the thermodynamically stable Cu–chelator complex, and by this enables the inhibition of ROS production in a reducing environment at physiological pH.